NASA Technical Memorandum 81262

Predicted and Experimental Steady and Unsteady Transonic Flows About a Biconvex Airfoil

Lionel L. Levy, Jr.

February 1981

NASA

NASA Technical Memorandum 81262

Predicted and Experimental Steady and Unsteady Transonic Flows About a Biconvex Airfoil

Lionel L. Levy, Jr., Ames Research Center, Moffett Field, California

NASA
National Aeronautics and
Space Administration

Ames Research Center
Moffett Field, California 94035

PREDICTED AND EXPERIMENTAL STEADY AND UNSTEADY TRANSONIC FLOWS ABOUT A BICONVEX AIRFOIL

Lionel L. Levy, Jr.

Ames Research Center

SUMMARY

Results of computer-code time-dependent solutions of the two-dimensional compressible Navier-Stokes equations and the results of independent experiments are compared to verify the Mach-number range for instabilities in the transonic flow field about a 14%-thick biconvex airfoil at an angle of attack of 0° and a Reynolds number of 7×10^6. The computer code predictions were made at Ames Research Center, and the experiments were conducted in a transonic, slotted-wall wind tunnel at the Royal Aircraft Establishment, Bedford, England. The computer code included an algebraic eddy-viscosity turbulence model developed for steady flows, and all computations were made using free-flight boundary conditions. All of the features documented experimentally for both steady and unsteady flows were predicted qualitatively; even with the above simplifications, the predictions were, on the whole, in good quantitative agreement with experiment. In particular, predicted time histories of shock-wave position, surface pressures, lift, and pitching moment were found to be in very good agreement with experiment for an unsteady flow. Depending upon the free-stream Mach number for steady flows, the surface pressure downstream of the shock wave or the shock-wave location was not well predicted.

NOMENCLATURE

C_l lift coefficient

C_m pitching-moment coefficient about the airfoil quarter chord

C_p pressure coefficient, $(p - p_\infty)/q_\infty$

c airfoil chord

M Mach number

p pressure

q dynamic pressure

Re_c Reynolds number based on airfoil chord and free-stream conditions

T temperature

t time

u velocity component in the x direction

x,y axes parallel and normal, respectively, to airfoil chord with origin at airfoil leading edge

ω circular frequency

Subscripts:

∞ free-stream conditions

rms root-mean-square value

t total conditions

Superscript:

* sonic conditions

INTRODUCTION

For a number of years Ames Research Center has been conducting companion programs of basic research in experimental and computational fluid dynamics for testing and guiding the development of turbulence modeling within regions of separated flows (ref. 1). One of these programs has contributed significantly to a renewed interest in high-Reynolds-number transonic flows, specifically the experimental documentation and computation of transonic flows about an 18%-thick circular arc airfoil (refs. 2-9). For this airfoil at an angle of attack of 0°, three distinctly different types of supercritical flows were documented experimentally for the first time in reference 3. Similar documentation at angles of attack was subsequently reported in reference 8. For a constant angle of attack and Reynolds number, and at progressively higher free-stream Mach numbers, the flow field about the airfoil can be (1) steady, with trailing-edge boundary-layer separation, (2) unsteady, with aerodynamically self-excited periodic oscillations in shock-wave location and intensity and in the location of boundary-layer separation, or (3) can be steady with shock-induced separation. It was demonstrated in reference 6 that two-dimensional computer codes for solutions of the Reynolds-averaged, compressible Navier-Stokes equations are capable of reproducing the time-dependent features of unsteady, transonic, turbulent separated flows, even if the code employs a simple algebraic eddy-viscosity turbulence model developed for steady flows.

An independent experimental study of the effect of thickness-to-chord ratio on the transonic Mach-number range for shock-induced periodic flows about biconvex airfoils at an angle of attack of 0° and at Reynolds numbers

up to 6×10^5 has been made by Mabey at the Royal Aircraft Establishment, Bedford, England (ref. 10). Based on the results of reference 10, the RAE decided to extend the study to Reynolds numbers up to 7×10^6. For this purpose a 14%-thick biconvex airfoil was selected to verify the expected Mach-number range for transonic-flow instabilities and to measure the chordwise distribution of oscillatory pressures. Furthermore, the results could provide additional experimental data against which to test the feasibility of the Ames Navier-Stokes-type computer code, used in reference 6, for predicting both steady and unsteady transonic, separated turbulent flows. Accordingly, NASA and RAE entered into an agreement in which Ames Research Center would compute three Navier-Stokes solutions to complement the experimental results given in reference 11. Using the results of reference 10 as a guide, one solution would be at a Mach number to verify an expected oscillatory flow and one solution each at lower and higher Mach numbers to verify expected steady flows.

This paper briefly describes the experimental and computational approaches to this joint study. Similarities and differences between the experiments and computations are noted, and computed and experimental results are compared to illustrate the current predictive capabilities of a two-dimensional computer program coded for the Reynolds-averaged, compressible Navier-Stokes equations and an algebraic eddy-viscosity turbulence model developed for steady flows.

APPROACH

Selection of the NASA/RAE-collaboration-agreement test conditions for comparisons of predicted and experimental results was based originally on the results of reference 10. Those results indicated that a 14%-thick biconvex airfoil at an angle of attack of 0° and at a Reynolds number of 6×10^5 experienced unsteady periodic flows in the Mach-number range from 0.81 to 0.85. From the trends with Reynolds number indicated in reference 8, one would expect similar transonic-flow instabilities over the same small Mach-number range at a Reynolds number of 7×10^6, the highest experimental Reynolds number attainable for the experiment (ref. 11). Accordingly, three sets of initial conditions were selected for the two-dimensional Navier-Stokes solutions. For a Reynolds number Re_c of 7×10^6, free-stream Mach numbers M_∞ of 0.80 and 0.86 were selected to verify expected steady flows; and an M_∞ of 0.83 was selected to verify an expected unsteady, oscillatory flow. The computations for these three cases were initiated at Ames Research Center before the experiments were begun at the RAE.

When the experiments were completed at RAE, the results indicated the desirability of changing M_∞ for the three computational cases because the experimental M_∞ range for periodic flows was found to be from 0.82 to 0.86. The free-stream conditions finally selected for comparison of predicted and experimental results are listed in table 1. Note that the computational free-stream conditions for the two steady-flow cases (M_∞ = 0.81 and 0.88) were changed to match the experiments. Computations at these M_∞'s were completed prior to receipt of experimental results. By the time the experiments were

TABLE 1.- FREE-STREAM CONDITIONS

	M_∞	$Re_c \times 10^{-6}$	T_t, °R
Computation	0.81	6.9	530
Experiment	0.81	6.9	530
Computation	0.83	7.0	500
Experiment	0.85	7.0	532
Computation	0.88	7.1	534
Experiment	0.88	7.1	534

completed and detailed unsteady-flow data obtained at $M_\infty = 0.85$, too much time had been invested in the original calculations at $M_\infty = 0.83$ to warrant a restart of this case, which exhibited an unsteady periodic flow. Other differences between the experiments and the computations are noted below.

Experiment

As stated in reference 11, an aluminum model of a 14%-thick biconvex airfoil — chord 300 mm, semispan 600 mm — was mounted from the center of one side wall of a 640-mm-high by 910-mm-wide RAE wind tunnel with slotted upper and lower test-section walls. Although this arrangement is technically a three-dimensional test setup, the flow was determined to be "two-dimensional" at the center of the semispan model where both the static and dynamic pressures were measured simultaneously in real time at 15 chordwise stations on both upper and lower surfaces of the airfoil. To insure a turbulent boundary layer over most of the airfoil at a Reynolds number of 7×10^6, carborundum transition trips were used at 2% chord on each surface. The ventilated test section was unchoked during tests at all Mach numbers.

Computations

Predictions of the flow field were made using a slightly modified version of the computer program described in reference 6. That program utilizes an explicit finite-difference method (refs. 2, 12, 13) to solve the time-dependent, two-dimensional, Reynolds-averaged form of the compressible Navier-Stokes equations; it incorporates the efficient numerical solver described in reference 14. The computer code also includes the additional equations for the turbulence model described in reference 6. The slight modifications referred to above include correction of the two subtle coding errors mentioned in reference 6, which earlier may have introduced numerical asymmetries. Also, the mesh size of the C-type computational domain was increased from 78×35 to 138×35 to provide more mesh points on the airfoil in the streamwise direction.

Detailed descriptions of the control volume, mesh, and boundary conditions are given in reference 15. For the present study, a 14%-thick circular-arc airfoil was impulsively started from rest at time zero at each of the computational free-stream conditions listed in table 1. The control volume, -6 and +8 chords in the x direction and ±6 chords in the y direction, was divided into a 138×35 mesh with 49 mesh points on each of the upper and lower airfoil surfaces. The flow-field development within this volume was followed in time until, nominally, it attained a steady state. For the present code, airfoil, and free-stream conditions, this required a time equivalent to the mean flow traveling about 8 chord lengths past the airfoil ($u_\infty t/c = 8$). Since the distributions of flow velocity through the slotted walls and the downstream static pressures were not available from the experiments, free-stream conditions were assumed at the far upstream and transverse boundaries, and zero gradients were assumed for all flow variables at the downstream boundary.

To avoid numerical difficulties associated with a sharp-edged airfoil and a C-type mesh, all computations were made for a 14%-thick circular arc airfoil modified for a 0.71% nose radius. This foreshortens an unmodified airfoil approximately 2% and does not affect results computed at an angle of attack of 0°. Consistent with the experiments of reference 11, turbulent boundary-layer flow was initiated over the airfoil at 2% chord.

RESULTS AND DISCUSSION

The computed results for the free-stream conditions listed in table 1 predicted the same general features of the flow fields observed in the corresponding experiments reported in reference 11. At $M_\infty = 0.81$ the flow field was steady with a strong shock wave and trailing-edge separation. At $M_\infty = 0.83$ the predicted flow field was unsteady, with periodic oscillations in shock-wave location and intensity and accompanying oscillations in the extent of boundary-layer separation. The same phenomena occurred on opposite surfaces of the airfoil 180° out of phase. This type of flow was observed experimentally at M_∞ between 0.82 and 0.86. At $M_\infty = 0.88$ the flow field was steady with a shock wave sufficiently strong to induce separation at the base of the shock wave, which extended downstream beyond the airfoil trailing edge. The two steady flow fields, in actuality, were pseudosteady. The shock-wave location and intensity, the location of boundary separation, and the pressure distributions did experience small variations about mean values in both the computations and the experiments.

Results of comparing details of the predicted and experimental data will be discussed separately for the steady and unsteady flows. To obtain root-mean-square values (rms) for the steady flows, predicted results for these cases were obtained from analyses of solutions computed over a time equivalent to 2 chord lengths of travel of the mean flow beyond that for which a solution is normally considered to have converged to a steady state. Because of the symmetry of the mean quantities determined over this time interval, results for the steady flow fields are presented for only half of the airfoil. Predicted results for the unsteady-flow case are from analyses of time histories

of solutions for four consecutive cycles of flow field oscillation (approximately 27 chord lengths of travel of the mean flow). Certainly more cycles are desirable; however, four are considered sufficient for purposes of the present comparisons.

Steady Flows

Predicted and experimental shock-wave locations and pressure distributions for $M_\infty = 0.81$ are shown in figure 1. The Mach contours in figure 1(a) indicate that the predicted shock wave is located less than 2% downstream of the actual shock wave. (Coalescence of the contours about the dashed sonic line indicate the formation of a shock wave -- the closer the contours, the stronger the shock wave). The same relative locations are indicated in figure 1(b) by the predicted and experimental jumps in the mean pressure distribution near $x/c = 0.7$. The mean pressure is predicted fairly well except over the last 20% of the airfoil. In the experiment, trailing-edge separation is reported to occur at $x/c = 0.87$ (ref. 11), while in the computations, separation occurs first at the base of the shock wave ($x/c = 0.7$) followed by reattachment and subsequent separation extending into the wake. The locations of reattachment and subsequent separation vary with time. An instantaneous example is indicated in figure 1(a) by the dotted line, which is the Mach contour defined for $u = 0$.

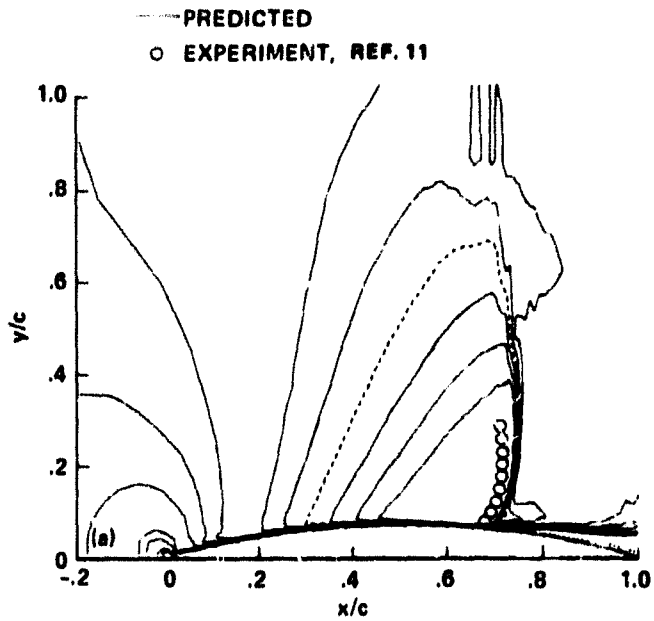

(a) Mean shock-wave location.

Figure 1.- Predicted and experimental shock-wave locations and pressure distributions, $M_\infty = 0.81$.

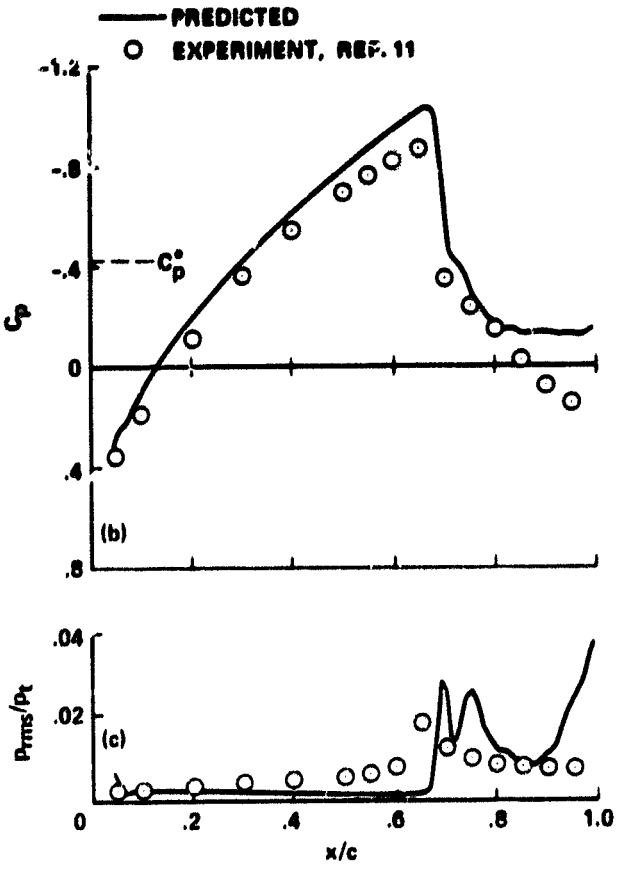

(b) Mean pressure.

(c) Rms pressure.

Figure 1.- Concluded.

The distribution of the rms values of the broadband pressure fluctuations are compared in figure 1(c). The results are qualitatively similar in that an increase in pressure fluctuations occurs at and immediately downstream of the shock wave. The magnitude of the increase, however, is overpredicted. This overprediction is attributed to an unsteadiness in the computed location of the reattachment and subsequent trailing-edge separation (noted above) that was not observed in the experiments.

The present computations, using free-flight upstream and transverse boundary conditions and zero-gradient-downstream boundary conditions, provide a good approximation to the flow field about this airfoil in the RAE slotted-wall test section at this M_∞. This result is consistent with the fact that the sonic line is computed to extend above the airfoil only to a y/c of 0.7 (fig. 1(a)), about 34% below the slotted walls located at y/c = 1.067. Differences in the predicted and experimental results noted in figure 1 are attributed to difficiencies in the turbulence model and a mismatch in the downstream boundary conditions.

Predicted and experimental shock-wave locations and pressure distributions for $M_\infty = 0.88$ are shown in figure 2. The predicted mean pressure is in excellent agreement with experiment ahead of the shock wave; however, as indicated by the Mach contours and pressure distributions in figures 2(a) and 2(b), respectively, the shock wave is predicted to be 13% farther downstream than in the experiment. Prediction of the nearly correct mean pressure level downstream of the shock wave is fortuitous. In the experiment, the shock wave was nearly normal (see fig. 2(a)), with separation at the base of the shock extending downstream into the wake. The same type of separation pattern was predicted by the calculations (see, e.g., the dotted line in fig. 2(a)); however, the separation emanates from the base of a calculated oblique shock wave.

The above-noted differences may be due, in part, to inadequate turbulence modeling; however, they are believed to result primarily from the mismatch in boundary conditions between the computations and the experiment. For example, the sonic line was computed to extend 2 chord heights above and below the airfoil – well beyond the location of the experimental slotted walls ($y/c = 1.067$). Although the location of the sonic line in the experiment is unknown, it is physically impossible that it extend much beyond the slotted wind-tunnel walls. Hence, there results a significant mismatch in the computational and experimental tunnel-wall boundary conditions. In addition, with zero-gradient-downstream boundary conditions there is no assurance that the flow parameters computed at the x/c of the wind-tunnel exit plane would match the experimental parameters at that location, had they been measured.

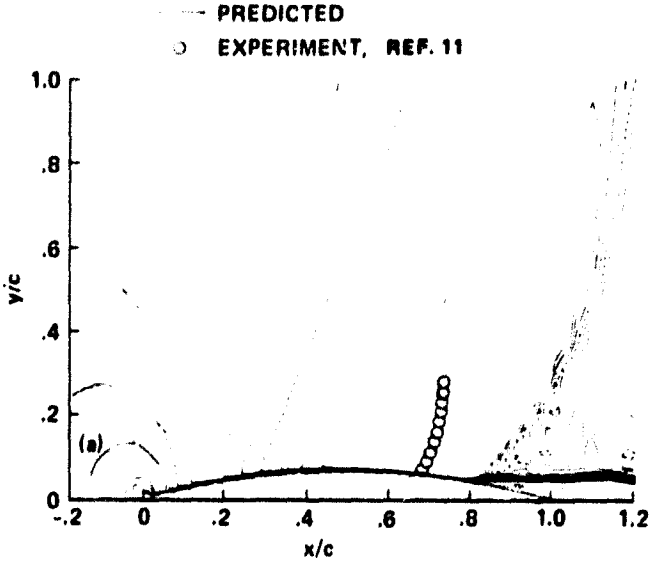

(a) Mean shock-wave location.

Figure 2.- Predicted and experimental shock-wave locations and pressure distributions, $M_\infty = 0.88$.

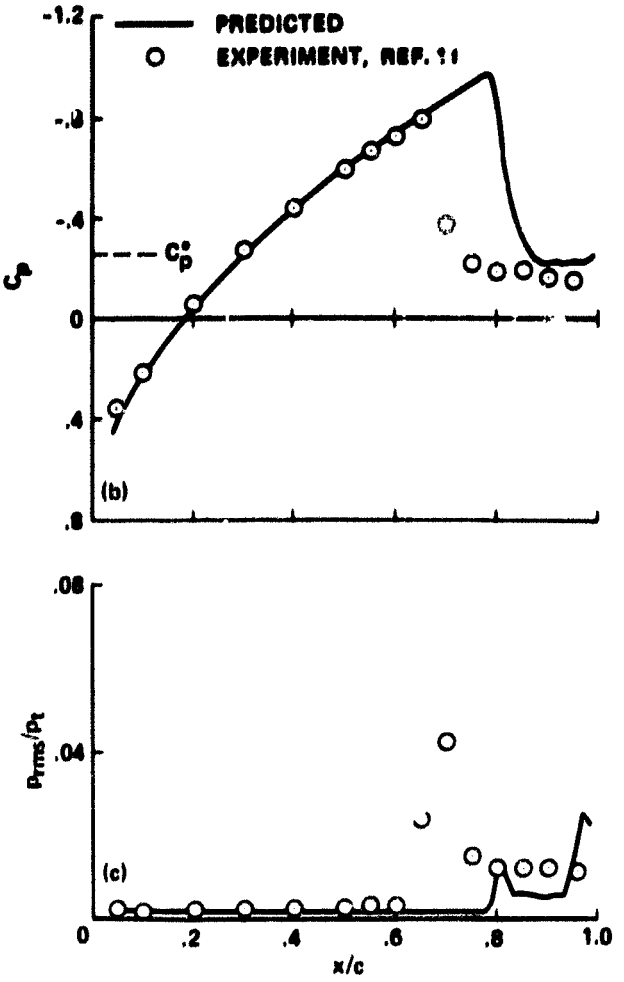

(b) Mean pressure.

(c) Rms pressure.

Figure 2.- Concluded.

Similar to the results at $M_\infty = 0.81$, the rms pressure fluctuations increase at and immediately downstream of the shock wave; however, at $M_\infty = 0.88$ the magnitude of the increase is underpredicted except near the trailing edge (fig. 2(c)). Overprediction at the trailing edge is attributed to an intermittent separation and reattachment of the boundary layer computed in this region but not observed in the experiments.

Unsteady Flows

As noted earlier, both the predicted and experimental flow fields exhibited periodic oscillations in shock-wave location and intensity, and in the

location of boundary-layer separation on opposite surfaces of the airfoil 180° out of phase. Although detailed comparisons can be made only between data available at different free-stream Mach numbers (see table 1), it is significant to note that the reduced frequency of the flow-field oscillation $\omega c/u_\infty$ was predicted to be 0.934; that reported in reference 11 at the same Mach number ($M_\infty = 0.83$) was 0.946.

Predicted and experimental pressure distributions for the unsteady-flow cases are compared in figure 3. In spite of the differences in M_∞ in the two sets of data, the experimental distributions are predicted quite well, particularly the distribution of rms pressure fluctuations in figure 3(b). For this case it is believed that the effect on the computations of the mismatch in boundary conditions is far less than that at $M_\infty = 0.88$. This is because examination of Mach-contour plots for a typical cycle of flow-field oscillation revealed that the sonic line on each side of the airfoil reached values of y/c that correspond to the location of the slotted tunnel walls during only 10% of the cycle. Also, subsequent comparisons of time histories of various aerodynamic quantities show good agreement between predicted and measured values.

Time histories of shock-wave location during a typical cycle of oscillation are compared in figure 4(b). Shown in figures 4(a) and 4(c) are plots of computed Mach contours selected to indicate the relative strength of the upper surface shock wave at its extreme positions during a cycle of motion. The "leaders" to figure 4(b) indicate the times during the cycle for each contour plot. In order to minimize the effect of different free-stream Mach numbers, the shock positions (and all subsequent time histories) are compared on the basis of chords traveled by the mean flow ($u_\infty t/c$). The experimental results were inferred from time histories of surface-pressure distributions. The predicted shock positions were defined as the values of x/c at the midpoint of the jump in surface pressure coefficient from 25 flow-field solutions used to define one cycle of oscillation. As an example, the data in figure 2(b) indicate a shock wave on the surface located at $x/c = 0.816$ where $C_p = -0.6$.

It was noted in reference 11, and is indicated in figure 4(b) that as the shock waves moved rearward they diminished in strength and at the most rearward locations were not visible in the high-speed shadowgraph movies. Although the Mach contours obtained during these portions of the cycle do indicate a definite sonic line similar to the dashed line shown above the airfoil in figure 4(a), it can be noted that the Mach-number gradient across the sonic line is much less (larger spacing in the streamwise direction) than when the shock wave is at the more forward chord stations (see, e.g., upper surface in figure 4(c)). In fact, values of the second derivative of the density (the quantity to which a shadowgraph system is sensitive), computed across the upper surface sonic line as far away from the surface as $y/c = 0.3$ for figure 4(a) was found to decrease by a factor of 27 within the first 10% of a chord above the airfoil compared with that for figure 4(c). This result indicates that the intensity of the shock wave does greatly diminish away from the

airfoil surface as it moves rearward in the computations and probably vanishes, as in the experiment; however, the unknown relationship is how the photosensitive emulsion of high-speed movie film would respond to the magnitude of the computed variation in density.

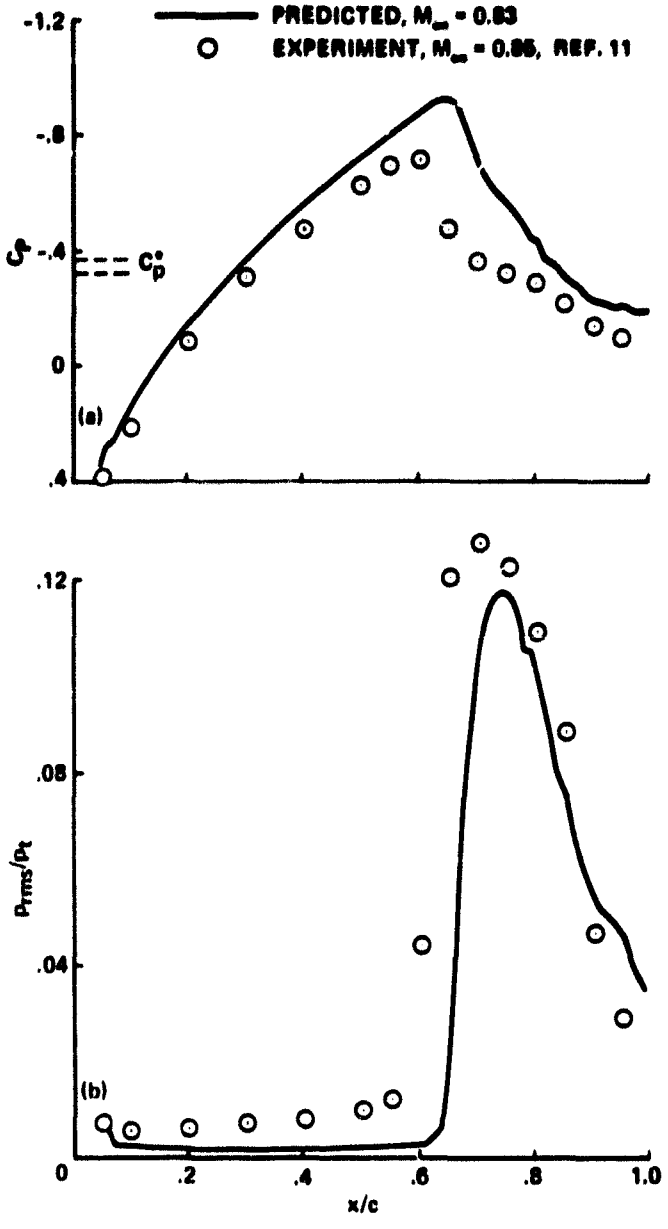

(a) Mean pressure.

(b) Rms pressure.

Figure 3.- Predicted and experimental pressure distributions for unsteady flows.

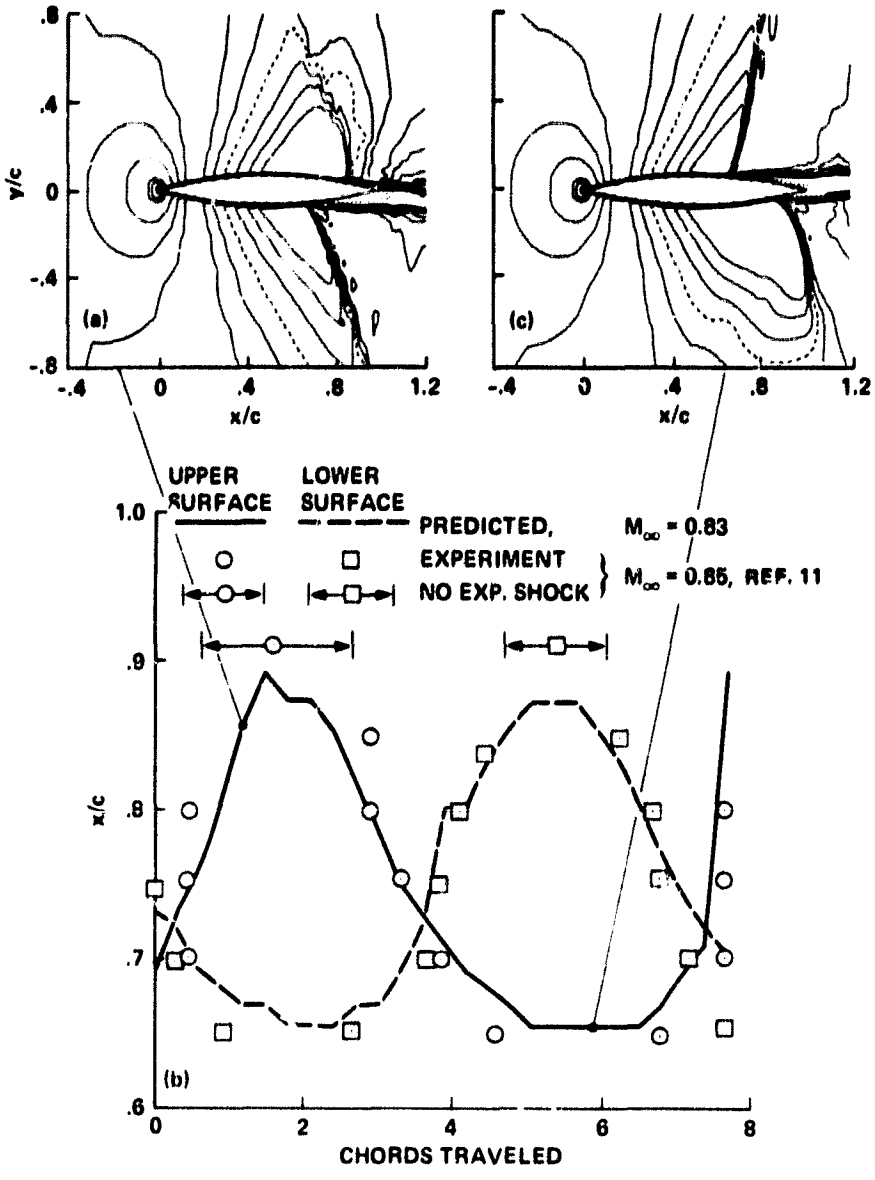

(a) Upper shock wave, rearward.

(b) Shock-wave locations.

(c) Upper shock wave, forward.

Figure 4.- Predicted and experimental shock-wave locations during a typical cycle of oscillation and selected Mach-contour plots.

Time histories of the pressure at four selected chord stations are compared in figure 5 for two cycles of oscillation. The waveform, frequency, and magnitude of pressure variations are predicted quite well at the more rearward x/c locations (figs. 5(c) and 5(d)) where the rms pressures are also better predicted. See, for example, figure 3(b) at x/c = 0.7 and 0.8. The most forward movement of the shock wave shown in figure 4(b) is to x/c = 0.65. In the experiment, weak pressure fluctuations propagate as far forward as x/c = 0.55, as shown in figure 5(a) and 5(b). In reference 11 these fluctuations are attributed to weak compression waves ahead of the main shock wave, which apparently are not present in the computations.

Even though the magnitude of the instantaneous surface pressures are overpredicted and underpredicted at different chord locations, the chordwise integration of instantaneous pressures generally overpredicts the magnitudes of the unsteady lift and pitching moment about the quarter chord. These predicted and experimental time histories are compared in figure 6 where it can be seen that the reduced frequency of oscillation is predicted quite well.

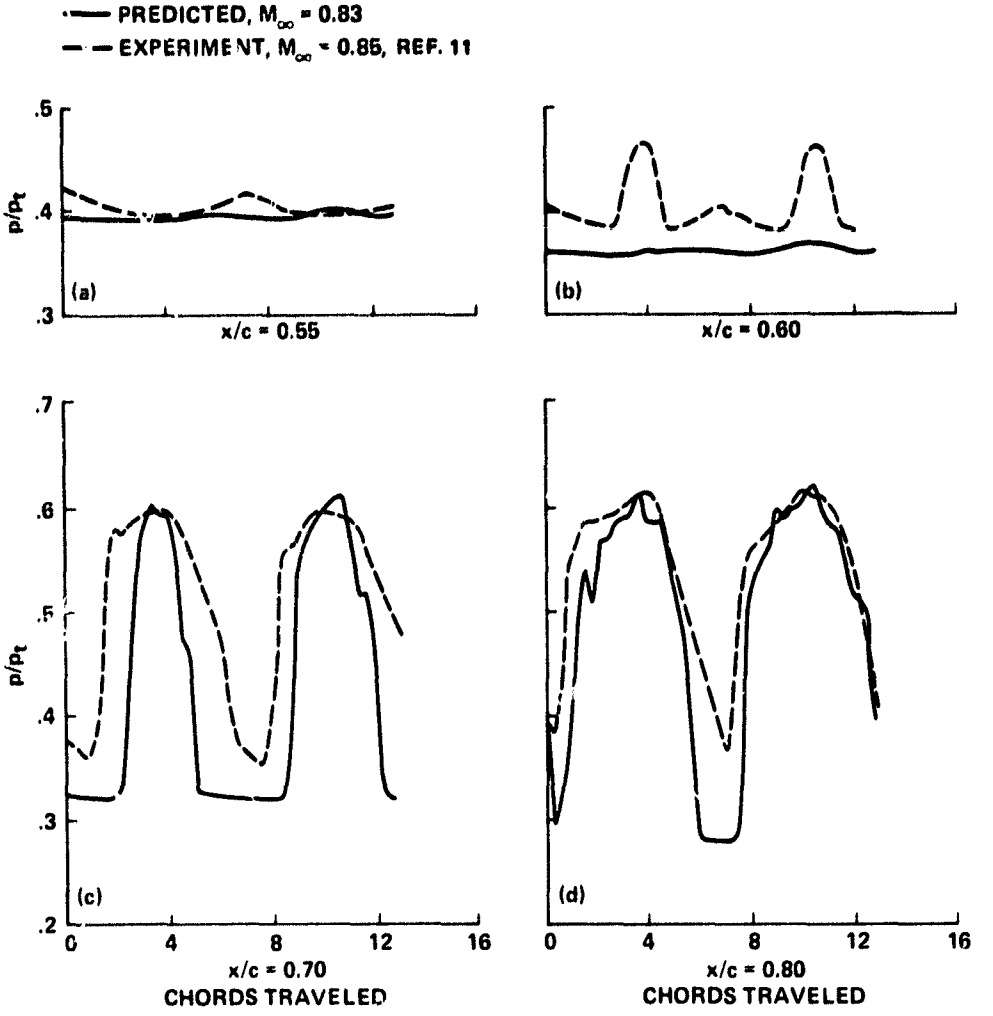

Figure 5.- Predicted and experimental surface-pressure time histories.

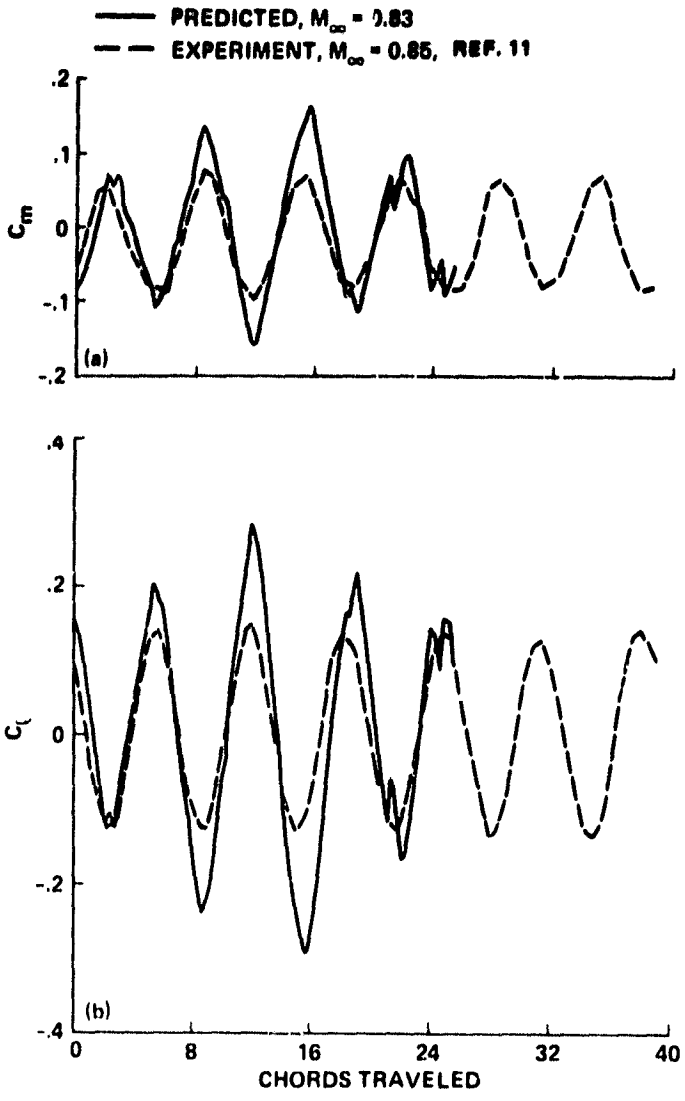

(a) Pitching moment.

(b) Lift.

Figure 6.- Predicted and experimental pitching-moment and lift time histories.

CONCLUDING REMARKS

A computer code for time-dependent solutions of the two-dimensional, Reynolds-averaged form of the compressible Navier-Stokes equations has been used at Ames Research Center to predict and compare results with experiments made at the Royal Aircraft Establishment, Bedford, England, to verify the Mach number range for instabilities in the transonic flow field about a

14%-thick biconvex airfoil at an angle of attack of 0° and a Reynolds number of 7×10^6. The experiments were conducted in a transonic wind tunnel with slotted upper and lower walls. The computer code included a simple algebraic eddy-viscosity turbulence model developed for steady flows, and all computations were made using free-flight boundary conditions. All of the features documented experimentally for both steady and unsteady flows were predicted qualitatively, and in many instances the predictions were in good quantitative agreement with experiment, even with the above simplifications.

At a free-stream Mach number of 0.81, where the characteristic features of the steady flow are a reasonably strong shock wave with boundary-layer separation near the trailing edge, the shock-wave location and the mean and rms pressure distributions were well predicted except over the last 20% of the airfoil. At a free-stream Mach number of 0.88, where the characteristic features of the steady flow are a shock wave sufficiently strong to induce a boundary-layer separation that extends from the base of the shock wave downstream into the wake, the predictions were not as accurate as they were at Mach number 0.81, particularly for the chordwise location of the shock wave. At $M_\infty = 0.88$ the predicted shock-wave location was 13% downstream of the experimental location and at $M_\infty = 0.81$ less than 2% downstream. This is believed to result from a greater effect on the computations of the mismatch in the boundary conditions when the sonic line in the flow field about the airfoil extends closer to the wind-tunnel walls at the higher free-stream Mach number.

Experimental unsteady flows were observed over a Mach-number range from 0.82 to 0.86 and were documented in detail at $M_\infty = 0.85$. These flows are characterized by periodic oscillations of the shock-wave location and intensity and in the location of boundary-layer separation on opposite sides of the airfoil 180° out of phase. Computations at a free-stream Mach number of 0.83 predicted the identical features. Locations of the shock waves and their intensity and frequency were accurately predicted. Time histories of the fluctuating pressures were in good agreement with experiment at all chordwise stations except for $0.5 < x/c < 0.7$. The computed mean and rms pressure distributions and time histories of the unsteady lift and pitching moment were in good agreement with experiment.

The results of comparisons of the predicted and experimental flow fields in the present study are sufficiently encouraging that in the near future a computational capability for predicting the Reynolds number, Mach number, and angle of attack at which airfoils can be expected to experience unsteady forces and for predicting the magnitude of those forces can be anticipated. Just how far into the future depends on progress in developing improved turbulence models for unsteady flows and on the availability of well-documented experiments — particularly for the boundary conditions.

REFERENCES

1. Marvin, J. G.: Experiments Planned Specifically for Developing Turbulence Models in Computations of Flow Fields Around Aerodynamic Shapes. AGARD-CP-210, Oct. 1976.

2. Diewert, G. S.: Numerical Simulation of High Reynolds Number Transonic Flows. AIAA, vol. 13, Oct. 1975, pp. 1354-1359.

3. McDevitt, J. B.; Levy, L. L., Jr.; and Diewert, G. S.: Transonic Flow About a Thick Circular-Arc Airfoil. AIAA, vol. 14, May 1976, pp. 606-613.

4. Deiwert, G. S.: Computation of Separated Transonic Turbulent Flows. AIAA, vol. 4, June 1976, pp. 735-740.

5. Rubesin, M. W.; Okuno, A. F.; Levy, L. L., Jr.; McDevitt, J. B.; and Seegmiller, H. L.: An Experimental and Computational Investigation of the Flow Field About a Transonic Airfoil in Supercritical Flow with Turbulent Boundary-Layer Separation. NASA TM X-73,157, 1976.

6. Levy, L. L., Jr.: Experimental and Computational Steady and Unsteady Transonic Flows About a Thick Airfoil. AIAA, vol. 16, June 1978, pp. 564-572.

7. Seegmiller, H. L.; Marvin, J. G.; and Levy, L. L., Jr.: Steady and Unsteady Transonic Flow. AIAA, vol. 16, Dec. 1978, pp. 1262-1270.

8. McDevitt, J. B.: Supercritical Flow About a Thick Circular-Arc Airfoil. NASA TM-78549, 1979.

9. Marvin, J. G.; Levy, L. L., Jr.; and Seegmiller, H. L.: On Turbulence Modeling for Unsteady Transonic Flows. AIAA, vol. 18, May 1980, pp. 489-496.

10. Mabey, D. G.: Oscillatory Flows from Shock-Induced Separations on Biconvex Aerofoils of Varying Thickness in Ventilated Wind Tunnels. Royal Aircraft Establishment TM Structures 969, Mar. 1980, AGARD SMP Conference, Sept. 1980.

11. Mabey, D. G.; Welsh, B. L.; and Cripps, B.: Periodic Flows on a 14% Thick Biconvex Wing at Transonic Speeds. Royal Aircraft Establishment, Unpublished Report, 1980.

12. Deiwert, G. S.: High Reynolds Number Transonic Flow Simulation. Lecture Notes in Physics, Vol. edited by Springer-Verlag, 1975, p. 132.

13. Baldwin, B. S.; MacCormack, R. W.; and Deiwert, G. S.: Numerical Techniques for the Solution of the Compressible Navier-Stokes Equations and Implementation of Turbulence Models. AGARD-LSP-73, Mar. 1975.

14. MacCormack, R. W.: An Efficient Numerical Method for Solving the Time-Dependent Compressible Navier Stokes Equations at High Reynolds Number. NASA TM X-73,129, 1976.

15. Deiwert, G. S.: On the Prediction of Viscous Phenomena in Transonic Flows. Project SQUID Workshop on Transonic Flow Problems in Turbomachinery, Monterey, Calif., Feb. 1975.